Phospholipase pPLAIIIα Increases Germination Rate and Resistance to Turnip Crinkle Virus when Overexpressed

Jin Hoon Jang, Ngoc Quy Nguyen, Bertrand Légeret, Fred Beisson, Yu-Jin Kim, Hee-Jung Sim, Ok Ran Lee

HAL Id: hal-03103329
https://hal.science/hal-03103329

Submitted on 11 Mar 2021

Phospholipase pPLAIIIα Increases Germination Rate and Resistance to Turnip Crinkle Virus when Overexpressed[1][OPEN]

Jin Hoon Jang,[a] Ngoc Quy Nguyen,[a] Bertrand Légeret,[b] Fred Beisson,[b] Yu-Jin Kim,[c] Hee-Jung Sim,[d,e] and Ok Ran Lee[a,2,3]

[a]Department of Applied Plant Science, College of Agriculture and Life Science, Chonnam National University, Gwangju 61186, Republic of Korea

[b]Biosciences and Biotechnologies Institute of Aix-Marseille, Commissariat à l'Énergie Atomique et aux Énergies Alternatives, Centre National de la Recherche Scientifique and Aix-Marseille University, Commissariat à l'Énergie Atomique et aux Énergies Alternatives Cadarache, 13108 Saint-Paul-lez-Durance, France

[c]Department of Life Science and Environmental Biochemistry, Pusan National University, Miryang, 50463, Republic of Korea

[d]Gyeongnam Department of Environmental Toxicology and Chemistry, Korea Institute of Toxicology, Jinju-si, 52834, Republic of Korea

[e]Center for Genome Engineering, Institute for Basic Science, Daejeon 34126, Republic of Korea

ORCID IDs: 0000-0003-0306-5283 (J.H.J.); 0000-0001-9995-7387 (F.B.); 0000-0003-2562-615X (Y.-J.K.); 0000-0002-5205-0080 (H.-J.S.); 0000-0002-6928-5863 (O.R.L.).

Patatin-related phospholipase As (pPLAs) are major hydrolases acting on acyl-lipids and play important roles in various plant developmental processes. pPLAIII group members, which lack a canonical catalytic Ser motif, have been less studied than other pPLAs. We report here the characterization of *pPLAIIIα* in Arabidopsis (*Arabidopsis thaliana*) based on the biochemical and physiological characterization of *pPLAIIIα* knockouts, complementants, and overexpressors, as well as heterologous expression of the protein. In vitro activity assays on the purified recombinant protein showed that despite lack of canonical phospholipase motifs, pPLAIIIα had a phospholipase A activity on a wide variety of phospholipids. Overexpression of *pPLAIIIα* in Arabidopsis resulted in a decrease in many lipid molecular species, but the composition in major lipid classes was not affected. Fluorescence tagging indicated that pPLAIIIα localizes to the plasma membrane. Although Arabidopsis *pplaIIIα* knockout mutants showed some phenotypes comparable to other *pPLAIIIs*, such as reduced trichome length and increased hypocotyl length, control of seed size and germination were identified as distinctive *pPLAIIIα*-mediated functions. Expression of some *PLD* genes was strongly reduced in the *pplaIIIα* mutants. Overexpression of *pPLAIIIα* caused increased resistance to turnip crinkle virus, which associated with a 2-fold higher salicylic acid/jasmonic acid ratio and an increased expression of the defense gene pathogenesis-related protein1. These results therefore show that *pPLAIIIα* has functions that overlap with those of other *pPLAIIIs* but also distinctive functions, such as the control of seed germination. This study also provides new insights into the pathways downstream of *pPLAIIIα*.

Lipases are a diverse group of hydrolases that break down acyl-lipids. Most of them hydrolyze the carboxyl ester bond between a fatty acid and the glycerol backbone, but lipase sequences diverge widely, and even the loose GXSXG esterase consensus for the catalytic Ser is not always present. Based on their preferred substrate, in vitro lipases are usually classified into triacylglycerol lipases, phospholipases, galactolipases, and others. However, many lipases often act in vitro on a variety of lipid classes, and the determination of their physiological role is not trivial. Genome analysis of Arabidopsis (*Arabidopsis thaliana*) has indicated that there are as many genes annotated as potentially involved in lipid breakdown as there are involved in lipid biosynthesis (Li-Beisson et al., 2013). Elucidation of the cellular function of the many putative plant lipases is thus a major challenge.

By hydrolyzing membrane phosphoglycerolipids, phospholipases participate in many aspects of plant cellular biology, such as signal transduction, cell growth regulation, and membrane remodeling in response to environmental stresses and lipid metabolism (Wang, 2001; Meijer and Munnik, 2003; Ryu, 2004; Matos and Pham-Thi, 2009; Scherer et al., 2010). Phospholipases of A-type (PLA) hydrolyze the carboxyl ester bond specifically at the *sn-1* or *sn-2* position of glycerophospholipids or in some cases at both positions. Plant PLA_2 families are classified into two groups: low-molecular–weight PLA_2s ($PLA_2\alpha$, $PLA_2\beta$, $PLA_2\gamma$, and $PLA_2\delta$) and patatin-related PLAs (pPLAs), the latter of which are homologous to the potato (*Solanum tuberosum*) tuber storage protein patatin. The pPLAs act on glycerogalactolipids as well as glycerophospholipids to release free fatty acids (FFAs) and the corresponding lysolipids (Lee et al., 2010; Scherer et al., 2010).

In Arabidopsis, the 10 members of the *pPLA* family have been classified into three groups based on gene

structure and amino acid sequence similarity: *pPLAI*, *pPLAII* (*pPLAIIα*, *pPLAIIβ*, *pPLAIIγ*, *pPLAIIδ*, and *pPLAIIε*), and *pPLAIII* (*pPLAIIIα*, *pPLAIIIβ*, *pPLAIIIγ*, and *pPLAIIIδ*; Holk et al., 2002; Scherer et al., 2010). Both *pPLAI* and *pPLAIIs* are involved in plant responses to pathogens, auxin signaling, and phosphate deficiency. Although the recently characterized pPLAIIIs lack the canonical catalytic Ser-containing motif GXSXG (Holk et al., 2002; Scherer et al., 2010), some pPLAIIIδ and pPLAIIIβ possess a lipase activity with broad substrate specificity (Li et al., 2011, 2013; Lin et al., 2011). In Arabidopsis, *pPLAIIIδ* is involved in plant response to auxin (Labusch et al., 2013). Moreover, in rice (*Oryza sativa*), *OspPLAIIIα* overexpression and knockout (*KO*) have an opposite effect on the expression of the growth repressor *SLENDER1* in the gibberellin signaling pathway (Liu et al., 2015). Overexpressors (*OE*) of *pPLAIIIs* display similar stunted growth patterns with additional functions, such as reduced cellulose content in *pPLAIIIβ-OE* (Li et al., 2011) or lignin in *PgpPLAIIIβ-OE* and *pPLAIIIα-OE* (Jang et al., 2019; Jang and Lee, 2020a, 2020b), and increased seed oil in *pPLAIIIδ-OE* (Li et al., 2013, 2015). Activation tagging of *pPLAIIIδ* (*STURDY*; Huang et al., 2001) also results in decreased longitudinal cell elongation and stunted growth, as observed in *pPLAIIIβ-OE*. The recessive rice mutant *dep3* with *OspPLAIIIδ* deficiency displays a dense and erect phenotype with short, wide epidermal cells (Qiao et al., 2011). A comparative proteomic analysis of *pPLAIIIδ-OE* and wild type has shown that one protein significantly differs between the *OE* and wild-type line, and it was identified as MICROTUBULE-ASSOCIATED PROTEIN18 (Zheng et al., 2014). Many physiological functions have been thus associated with *pPLAIIIs* in Arabidopsis or other plants, but the molecular pathways involved mostly remain to be elucidated.

To further shed light on the function of pPLAIIIα, we studied the activity of the recombinant protein in vitro, characterized overexpression and *KO* mutants in Arabidopsis at physiological and molecular levels, and performed lipidomic analyses.

RESULTS

Despite Lacking Canonical Motifs, pPLAIIIα has Retained Lipase Activity

Arabidopsis *pPLAIIIα* (At2g39220) was represented by a single gene encoding a protein of 499 amino acids with a predicted pI of 6.24 and a molecular mass of 54.5 kD. Like all Arabidopsis pPLAIII proteins, pPLAIIIα lacked the Ser of the putative Ser-Asp catalytic dyad because Ser present in the canonical GxSxG motif was replaced with G (Fig. 1A). However, the second residue of the putative catalytic Ser-Asp dyad, Asp, was present in the DGG motif. In addition, it can be noted that the phosphate or anion binding element DSGGXXG was not completely conserved in the pPLAIIIα protein because the second Gly was replaced with Ser.

Arabidopsis pPLAIIIα thus lacked the canonical phospholipase motif for the catalytic Ser found in other characterized pPLAIIIs and one could question whether this protein really possessed phospholipase activity. The recombinant pPLAIIIα protein His-tagged at the C-terminal end was therefore expressed in *Escherichia coli* and purified (Supplemental Fig. S1). In vitro enzymatic assays showed that the His-tagged pPLAIIIα had an acyl-ester hydrolase activity on each of the four major Arabidopsis phospholipid classes, with a slightly higher activity on phosphatidic acid (PA) than on phosphatidylcholine (PC), phosphatidylethanolamine (PE), or phosphatidylglycerol (PG; Fig. 1C).

Taken together, these results show that pPLAIIIα is a noncanonical phospholipase A that hydrolyzes various phospholipids in vitro.

Spatial and Temporal Expression Patterns of *pPLAIIIα*

To determine the expression pattern of *pPLAIIIα* in Arabidopsis, we generated *PropPLAIIIα::GUS* transformants using 2,087 bp upstream from ATG with 15-bp coding sequence (total 2,105 bp). The GUS reporter gene was expressed in most organs including inflorescences, flowers, siliques, stems, and leaves (Fig. 2) but displayed further distinct spatial or temporal expression patterns compared to other *pPLAIIIs* promoters (Dong et al., 2014). *pPLAIIIα* was highly expressed in roots, with greater restriction in the vasculature and meristematic zones of the lateral roots (Fig. 2, A and C–F). In germinating seeds, GUS activity was observed in embryo cotyledons and vasculature of roots during testa rupture and radical emergence (Fig. 2, C and D). Vasculature expression in sepals and petals was also observed in whole flower organs (Fig. 2B). In cotyledons and true leaves, stomata expression was restricted in the inner wall of the guard cell region (Fig. 2G).

Figure 1. Distinctive conserved motifs of pPLAIIIα and its lipase activity. A, Alignment of pPLAIIIα with other pPLAIIIs and two pPLAIIs from Arabidopsis. Amino acid sequences were analyzed using the pairwise sequence alignment program ClustalW (http://www.clustal.org/clustal2/). Multiple sequence alignment was performed using the program BioEdit (v.7.1.9; https://bioedit.software.informer.com/7.1/). B, Immunoblot analysis of recombinant pPLAIIIα protein using anti-6× His tag antibody on *E. coli* purified recombinant proteins. C, In vitro enzymatic assay of recombinant pPLAIIIα protein using a NEFA kit. pPLAIIIα fusion protein and 0.5 mM of each substrate (16:0-18:1 PA, PC, PE, and PG) were incubated at 30°C for 60 min. Data represent the mean ± SE of four independent biological replicates. Data were analyzed by one-way ANOVA. Means with different lowercase letters represent significantly different ($P < 0.05$), according to Scheffe's test.
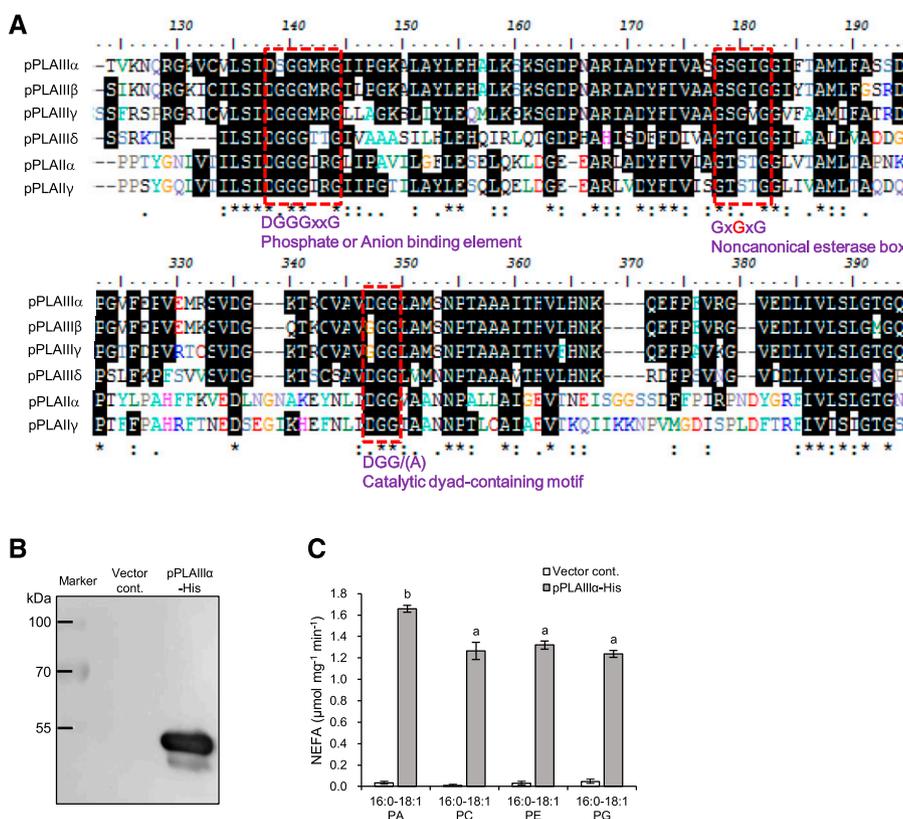
PropPLAIIIα::GUS was expressed highly in hypocotyls elongating in the darkness compared with those grown in the light (Fig. 2H). Cross-sectional images of stems indicate strong expression of *pPLAIIIα* in the xylem and phloem (Fig. 2I). Strong expression was also observed in the hydathodes of young leaves and trichomes (Fig. 2J). Overall, GUS expression was observed in all organs, with more restriction in the vasculature.

KO, OE, and Subcellular Localization of Arabidopsis *pPLAIIIα*

To study the function of *pPLAIIIα*, we performed gain- and loss-of-function experiments in Arabidopsis. We first isolated homozygous transfer DNA–insertion mutants for *pPLAIIIα* (Fig. 3A). In addition, the full-length genomic DNA sequence of Arabidopsis *pPLAIIIα* was overexpressed in Arabidopsis under the control of the 35S promoter with yellow fluorescence protein (YFP)- or monomeric red fluorescent protein (mRFP)-tagging at the C-terminal end. Immunoblotting using mRFP antibody detected expected size bands only visible in *OE* lines but not in KO lines (Fig. 3B). Both C-terminal YFP and mRFP tagging showed that pPLAIIIα localized to plasma membranes (PMs) in root cells (Fig. 3, C and D). The fluorescence signal of PM was separated from the cell wall, indicating its signal is not wall-associated (Fig. 3D). Quantification of *pPLAIIIα* transcript levels in four independent homozygous *OE* lines

(Fig. 3E) showed that *pPLAIIIα* was overexpressed very strongly in line 6 (440-fold), line 7 (420-fold), and line 13 (800-fold), and moderately in line 8 (5-fold). No transcripts were detected for two transfer DNA insertion lines in *pPLAIIIα*, indicating that they were *KO* mutants (Fig. 3E). Transcript expression levels corresponded to protein levels (Fig. 3B). Complementation lines (*pPLAIIIα-COM*) generated by crossing each *OE* line in the *KO* line 1 background (SAIL830G12) still displayed overexpression of *pPLAIIIα* but compromised where line 7 overexpressed 87-fold and line 13, 94-fold. This complementation result could be caused by overexpressing using the 35S promoter. Interestingly, transcripts for the closely related *pPLAIIIβ* (72% identity with *pPLAIIIα*), *pPLAIIIγ* (56%), and *pPLAIIIδ* (34%; Supplemental Fig. S2) were slightly modulated by the expression level of *pPLAIIIα* (Supplemental Fig. S3). In seedling stages (Fig. 3F), the hypocotyl length of the *pplaIIIα* mutants was longer than that of controls, but *OE* lines were shorter than controls (Fig. 3G). The root lengths were only shorter in two of the *OE* lines and unaltered in the *KO* mutant lines (Fig. 3H). Both *OE* lines 6 and 7 could be considered as ectopic lines with similar levels of expression, and *OE* line 13 was the most highly expressing line. However, *OE* line 8 was the most moderate line that was perfectly complemented in *KO* line 1 (Fig. 3, G and H). From the seedling stages, all *OE* lines displayed stunted and dwarf phenotypes with thicker cotyledons (Fig. 3F),
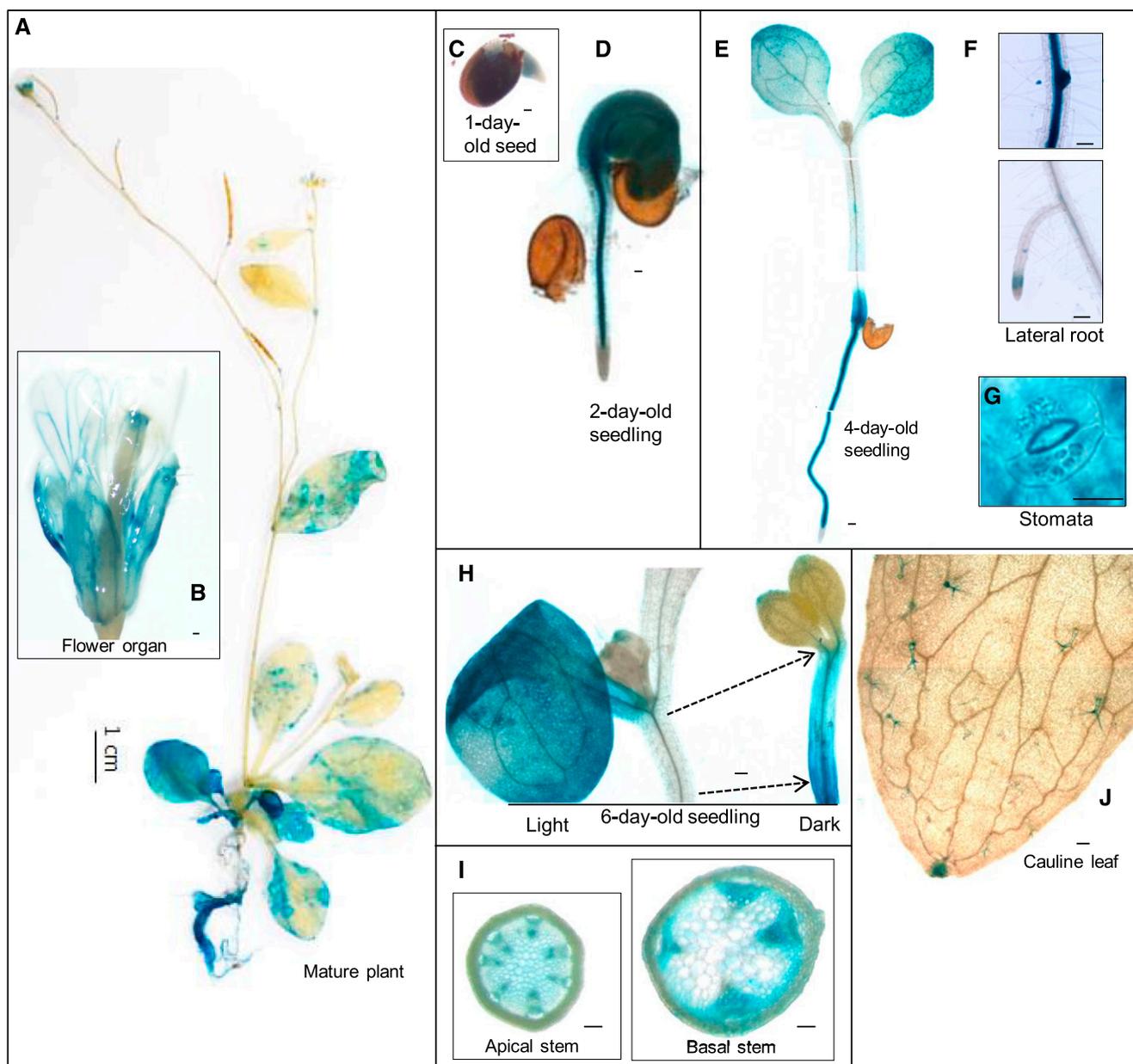
Figure 2. Spatial and temporal gene expression patterns of *pPLAIIIα* in Arabidopsis. Histochemical analysis of GUS expression harboring *PropPLAIIIα::GUS* at different developmental stages. A to J, GUS expression in a fully grown plant (A), a floral organ (B), a 1-d-old seedling (C), 2-d-old seedlings (D), 4-d-old seedlings (E), the vasculature of the roots and the meristematic zone of the lateral root (F), the inner cell wall of a guard cell (G), the light- and dark-dependent expression in 6-d-old seedlings (H), the vasculature of the apical and basal stem (I), and the mature cauline leaf (J). All images were brightness-adjusted. Scale bars = 100 μm.

which were also confirmed in the subsequent growth stages.

Lipidomics Reveal a Wide Range of Acyl-Lipids Are Decreased in *pPLAIIIα-OE* on a Seedling-Weight Basis

To determine which lipid molecular species may be affected in the knockout or overexpressor plants, total lipids were extracted from seedlings of a *pplaIIIα*

mutant and two strong *pPLAIIIα-OE* lines, and 115 molecular species of acyl-lipids (including phospholipids, galactolipids, and sulfolipids) were analyzed by liquid chromatography tandem mass spectrometry (LC-MS/MS; Fig. 4; Supplemental Figs. S4 and S5).

In the *pplaIIIα KO* mutant, analysis of the lipid molecular species did not reveal significant differences, including in the phospholipid species potentially localized to the PM (Fig. 4C; Supplemental Fig. S4). In *OE* lines, total acyl-lipids were reduced ~25% on a seedling
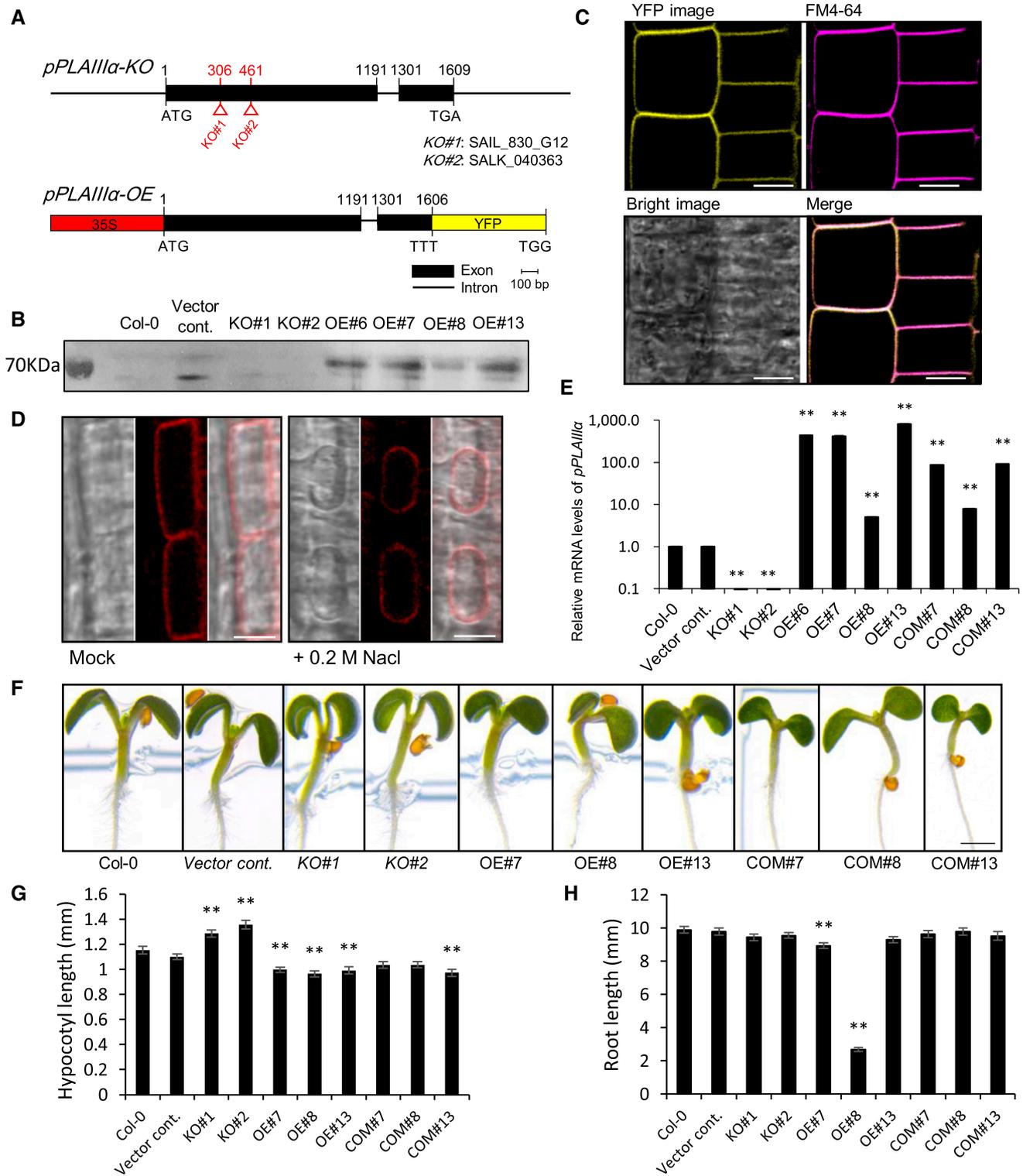
Figure 3. KO, OE, and complementation lines for *pPLAIIIα* in Arabidopsis. A, The transfer DNA insertion sites in two Arabidopsis *pplalllα KO* mutants and a diagram showing the OE construct of *pPLAIIIα* (*pPLAIIIα-OE*) under the control of the 35S promoter with YFP or mRFP fusion at the C terminus. B, Immunoblotting of mRFP-tagged pPLAIIIα from Col-0, vector control, *KO*, and *OE* plants. After SDS-PAGE separation, protein was immunoblotted with anti-mRFP antibody. C, Subcellular localization of pPLAIIIα-YFP in the PM merged with FM4-64. Scale bars = 10 μm. D, Plasmolysis of root epidermal cells of the pPLAIIIα-mRFP with 0.2 M of NaCl for 1 min. Scale bars = 10 μm. E, Transcript levels of *pPLAIIIα* genes in the controls, *KO, OE,* and complementation (*COM*) lines as measured by RT-qPCR. $n = 3$. F, Phenotypes of 4-d-old seedlings. Scale bar = 1 cm. G and H, The hypocotyl length

fresh weight (FW) basis in both lines compared to the vector control (Fig. 4A). Significant decreases were observed in many lipid classes (Fig. 4B). This included major phospholipid classes, such as the mostly extraplastidial PC and PE and the plastidial/ mitochondrial PG, the minor phospholipid class PA, and some purely plastidial lipid classes such as the galactolipid monogalactosyldiacylglycerol (MGDG) and digalactosyldiacylglycerol (DGDG), and the sulfolipid class sulfoquinovosyldiacylglycerol (SQDG). For plastidial lipids, both "prokaryotic" species (C18/ C16, i.e. C34) and "eukaryotic" species (C18/C18, i.e. C36) were affected (Fig. 4C). The reduction was almost evenly distributed among all glycerolipid classes, and the lipid class composition was thus not significantly affected in the two *OE* lines (Supplemental Fig. S5). In the *OE* lines, a reduction was seen in most of the major molecular species (Fig. 4C) and the minor ones also (Supplemental Fig. S4). The PA class appeared to be particularly impacted with almost all molecular species of PA reduced by 30% to 50% (Fig. 4C). Lysolipids were not significantly changed, except for the lysoMGDG and lysoPG species, which were significantly reduced in both *OE* lines. No accumulation of a particular FFA species (Fig. 4C) or of total FFAs (Fig. 4B) was measured in the *OE* lines.

In conclusion, lipidomic analyses show that total lipid amount per FW and the composition in glycerolipid molecular species remained unchanged in the *pplaIIIα KO* mutant. In *OE* lines, FFAs did not accumulate, and composition in glycerolipid classes was not significantly changed in either of the *OE* lines.

pPLAIIIα Expression Level Affects the Size and Shape of Many Cells and Organs

Transversely expanded cell morphology with altered longitudinal cell elongation has been previously reported after the overexpression of *pPLAIIIβ* and *pPLAIIIδ* (Huang et al., 2001; Li et al., 2011, 2013; Dong et al., 2014). We thus investigated the possible role of *pPLAIIIα* in Arabidopsis growth and development by performing a detailed phenotypic analysis of several organs in *OE* and *KO* lines for *pPLAIIIα*. Overall, *OE* plants were, on average, 9 cm shorter in strongly expressing lines compared with the controls (Fig. 5A). The size of the rosette leaves decreased, and the number of leaves decreased with increasing *pPLAIIIα* expression (Fig. 5, B and C). In three strong *pPLAIIIα-OE* lines (lines 6, 7, and 13), leaves were 1.7-fold thicker and contained more water (3%) on average (Fig. 5, D and E). A reduction in organ size in *pPLAIIIα-OE* lines was also clearly seen in other organs such as flowers and siliques

(Fig. 5, F and G), hypocotyls (Fig. 3G), roots (Fig. 3H), and petioles (Supplemental Fig. S6).

At the cellular level, when *pPLAIIIα* was overexpressed, longitudinal elongation patterns from cells were reduced as observed in stems (Fig. 5H) and flowers (Fig. 5F; Supplemental Fig. S7A); conversely, stem cells expanded transversely (Fig. 5I). However, the number of cells per stem cross section was similar in wild-type, *KO, OE,* and *COM* lines (Fig. 5J). Here, *OE* line 8 was again solely complemented in the *KO* background, and *OE* line 13 displayed partial complementation in stem thickness (Fig. 5I). The effect of *pPLAIIIα* overexpression on cell size and shape was also observed on trichomes (Supplemental Fig. S7, B and C) and pollen grains (Fig. 5K). Trichomes are predominantly three-branched on the adaxial surfaces of the rosette and cauline leaves of wild type (Higginson et al., 2003). The overall trichome size was strongly reduced in *pPLAIIIα-OE* (Supplemental Fig. S7, B and C), and a greater number of two-branched trichomes were observed compared with that in control (Supplemental Fig. S7B). While overexpression of *pPLAIIIα* had a strong effect on the sizes of many organs, silencing of the gene did not produce drastic effects in Arabidopsis plants. However, some differences occurred in *KO* mutants compared with Col-0, including an increase in length of hypocotyls (Fig. 3, F and G) and petioles (Supplemental Fig. S6). This observation suggests the possible involvement of *pPLAIIIα* in hormonal growth control by auxin, ethylene, and gibberellin that is essential for hypocotyl and petiole elongation (de Wit et al., 2016; Yang and Li, 2017) in wild-type plants.

pPLAIIIα-OE Is Involved in the Control of Seed Size and Germination

An exception to the reduction in organ size in *OE* lines occurred in seeds, which increased in width without alteration in length (Fig. 6, A and B). Consistently, seed weight increased 23% in *pPLAIIIα-OE* (line 13) and decreased 10% in *KO* mutants (Fig. 6C), thus showing that *pPLAIIIα* is involved in seed development in wild-type plants. In highly overexpressing *OE* lines, it was clear that the increased seed weights were at the expense of seed number per silique (Fig. 6D).

The fact that seed weights decreased in *KO* mutants prompted us to check seed germination rates (Zhong et al., 2016) and kinetics. After 20 h in the light, *KO* mutants showed 19% lower germination rates than the control, and the *OE* line showed a 10% greater germination rate on average (Fig. 6E). However, all *KO* seeds germinated by 30 h, which indicated that the germination rate was not affected, but that germination was

---

Figure 3. (*Continued.*)
(G) and root length (H) of the controls, for the *KO, OE,* and *COM* lines. *n* = 19 to 43. In E, G, and H, data represent the mean ± SE (SE) of independent replicates. Asterisks indicate significant difference compared with the controls using Student's *t* test (*$P < 0.05$ and **$P < 0.01$). Col-0 and an empty vector line were used as control for mutant and *OE* lines, respectively.
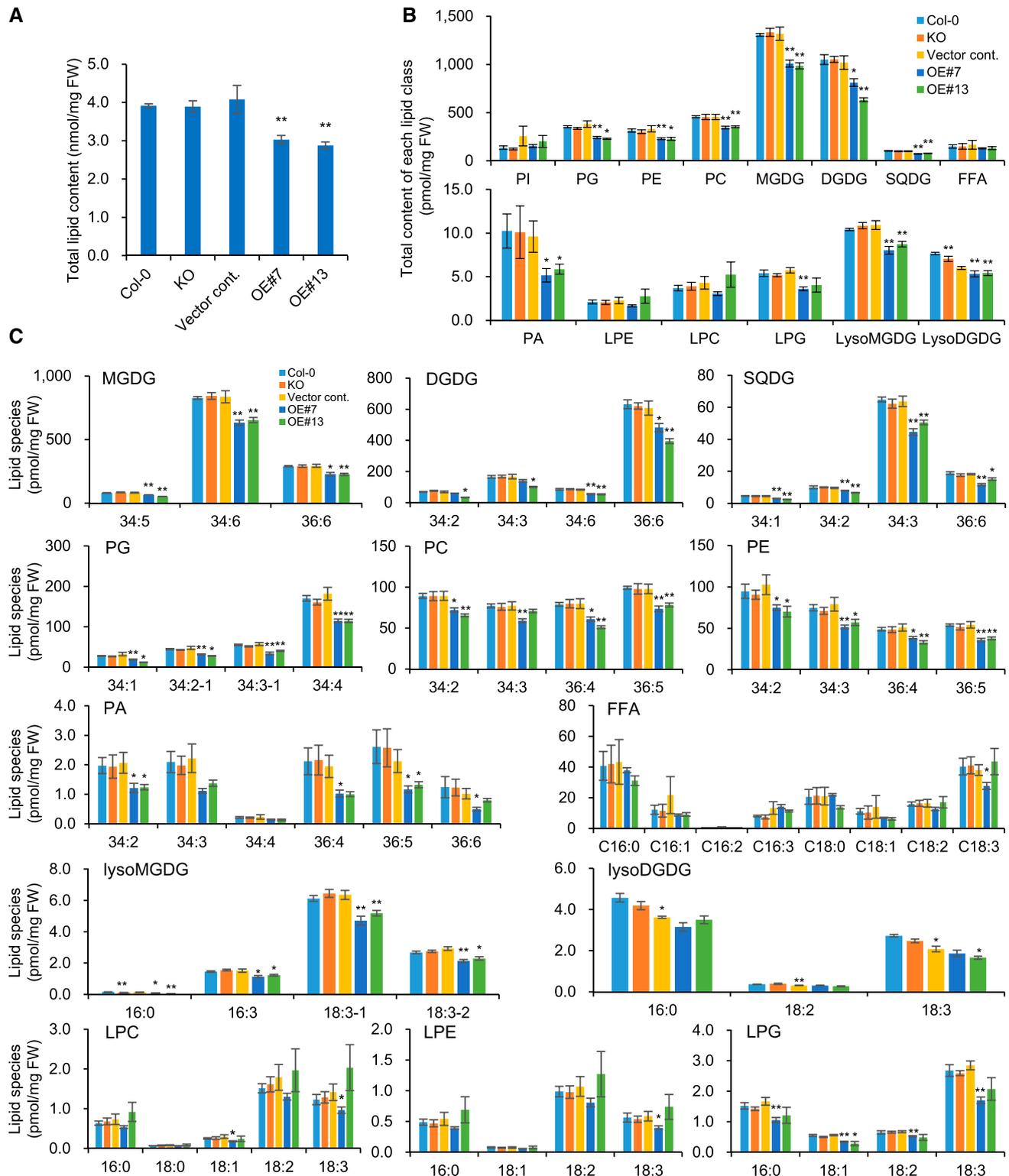
Figure 4. Total lipid content and abundance of lipid molecular species in *OE* and *KO* lines. A to C, Total lipid content (A), total content of each lipid class (B), and major lipid molecular species content (C) in *OE* and *KO* lines. Each molecular species of acyl-lipid was identified and quantified using UPLC-MS/MS in the *KO* mutant and *OE* lines compared with the controls. Values were normalized by FW of rosette leaves analyzed. Data represent the mean ± sᴇ of three (controls) to six (*KO* and *OEs*) independent biological replicates. Asterisks indicate significant differences using Student's *t* test (**P* < 0.05 and ***P* < 0.01) compared with the controls. Molecular species are indicated as the total number of carbon atoms in acyl chains: the total number of double bonds.

delayed compared to that in wild type. Treatment with gibberellic acid (GA)$_3$ did not alter the germination substantially (Fig. 6F). Because antagonism between abscisic acid (ABA) and GA plays a key role in controlling seed germination (Koornneef et al., 2002), we quantified ABA in dry seeds. ABA content increased in the mutant compared to the wild type (Fig. 6G). Altogether, the data suggest that the *KO* of *pPLAIIIα* delays the initial germination rate by changing endogenous GA and ABA biosynthesis.

Transcript Levels of Ethylene and GA Biosynthesis Genes Increased during *pPLAIIIα-OE* Seed Imbibition

The antagonistic effects of ethylene and ABA in the regulation of seed germination have also been extensively studied (for review, see Corbineau et al., 2014). Increased ethylene production is associated with an accumulation of ACC oxidase (*ACO*) transcripts (Corbineau et al., 2014). *ACO1* and *ACO2* are the major *ACO*s involved in ethylene synthesis. *ACO1*, *ACO2*, and *ACO4*, which exhibit *ACO* activity (Gómez-Lim et al., 1993; Linkies et al., 2009; Park et al., 2018), were all upregulated in *OE* lines, whereas *ACO1* and *ACO4* expression decreased in *KO* lines (Fig. 7A). Numerous data also suggest that ethylene stimulates seed germination by affecting GA biosynthesis (Corbineau et al., 2014). To uncover a possible role of bioactive GA biosynthesis, we analyzed expression of four GA oxidase genes. *GA20ox* and *GA3ox* encode enzymes that catalyze bioactive gibberellin biosynthesis, whereas *GA2ox1* and *GA2ox2* are involved in the conversion of bioactive gibberellins into an inactive form. Two *GA2oxs* were upregulated 1.4-fold in *KO* lines, whereas *GA20ox1* was upregulated 1.3-fold and *GA2ox2* was downregulated 0.6-fold in the *OE* lines (Fig. 7B). These data explain that the faster germination in *OE* lines might be due to more active forms of GA and increased levels of ethylene.

OE of *pPLAIIIα* Delayed Senescence by Reducing ROS

Suppression of the PA-generating *PLDα1* leads to reduced superoxide synthesis, and addition of exogenous PA to leaves promotes reactive oxygen species (ROS) production (Sang et al., 2001). Besides, in several plant systems, minor lipid PA content has been studied in relation to stress responses (Wang et al., 2006) through the modulation of ROS (Hong et al., 2008). Therefore, we decided to monitor hydrogen peroxide (H$_2$O$_2$) levels in 8-week-old mutant and *OE* lines (Fig. 8A) using 3,3-diaminobenzidine tetrahydrochloride

(DAB) staining (Fig. 8B). DAB is oxidized by H$_2$O$_2$ in the presence of heme-containing proteins to generate a dark-brown precipitate (Thordal-Christensen et al., 1997). In *OE* lines, leaves were greener in 8-week-old plants, when the leaves of wild-type plants had already become chlorotic (Fig. 8A). All plant leaves were green up to 28 d, but the levels of H$_2$O$_2$ were lower when *pPLAIIIα* was highly expressed, as observed in the *OE* lines compared with the wild type (Fig. 8B) after DAB staining. To confirm that the delayed senescence was caused by *pPLAIIIα*, we analyzed the expression of a representative downstream gene, *SENESCENCE-ASSOCIATED GENE12* (*SAG12*), which encodes a Cys protease (Lohman et al., 1994) upregulated during senescence. Expression of *SAG12* was 10-fold lower in four strong *OE* lines (Fig. 8C), which shows that high expression of *pPLAIIIα* retards senescence. By contrast, expression of *SAG13*, which may be induced by stress or cell death, was only slightly increased in two of the four *OE* lines analyzed (Fig. 8D).

OE of *pPLAIIIα* Confers Turnip Crinkle Virus Resistance by Altering Salicylic Acid and Jasmonic Acid Contents

OE of phospholipase activity by SOBER1 reduces PA levels and suppresses plant immunity to the bacterial effector AvrBsT (Kirik and Mudgett, 2009). However, a plant immunity study focusing on virus relative to the level of PA has not been previously reported. Considering that plant viruses are pathogens associated with major threats, resistance to turnip crinkle virus (TCV) in Arabidopsis, which is one of the few manipulative plant-virus systems, was tested in mutant and *OE* lines (Fig. 9). Formation of the hypersensitive response (HR) was visible in TCV-inoculated plant leaves 3-d postinoculation (DPI; Fig. 9, A and B) and in inflorescences at 12 DPI (Supplemental Fig. S8A), with the most severe effects in the *KO* mutant. Only highly expressing *pPLAIIIα-OE* (line 13) displayed an intact inflorescence (Fig. 9B). These phenotypes were consistent with the corresponding patterns of TCV gene expression, whereby the relative gene expression dramatically decreased in *OE* line 13 and increased in the *KO* mutant (Fig. 9C; Supplemental Fig. S8B). After TCV infection, several defense genes, such as pathogenesis-related protein1 (*PR1*), *PR2*, and *PR5*, are expressed, and salicylic acid (SA) accumulates (Kachroo et al., 2000). To determine whether this mechanism could be involved in higher virus resistance of *pPLAIIIα-OE*, the gene expression patterns of two representative SA and jasmonic acid (JA) pathway genes were analyzed using leaves at 3 DPI (Fig. 9, D and E). *PR1* was upregulated in both *OE* lines, whereas *PDF1.2* expression significantly

---

Figure 4. (*Continued.*)
Dashes (e.g. 18:3-1 and 18:3-2) indicate two species with the same mass and fragmentation pattern but with different retention times. For MGMG, DGDG, SQDG, PG, PC, and PE classes, only the three or four major species are shown. Minor species for these lipid classes are shown in Supplemental Figure S4.
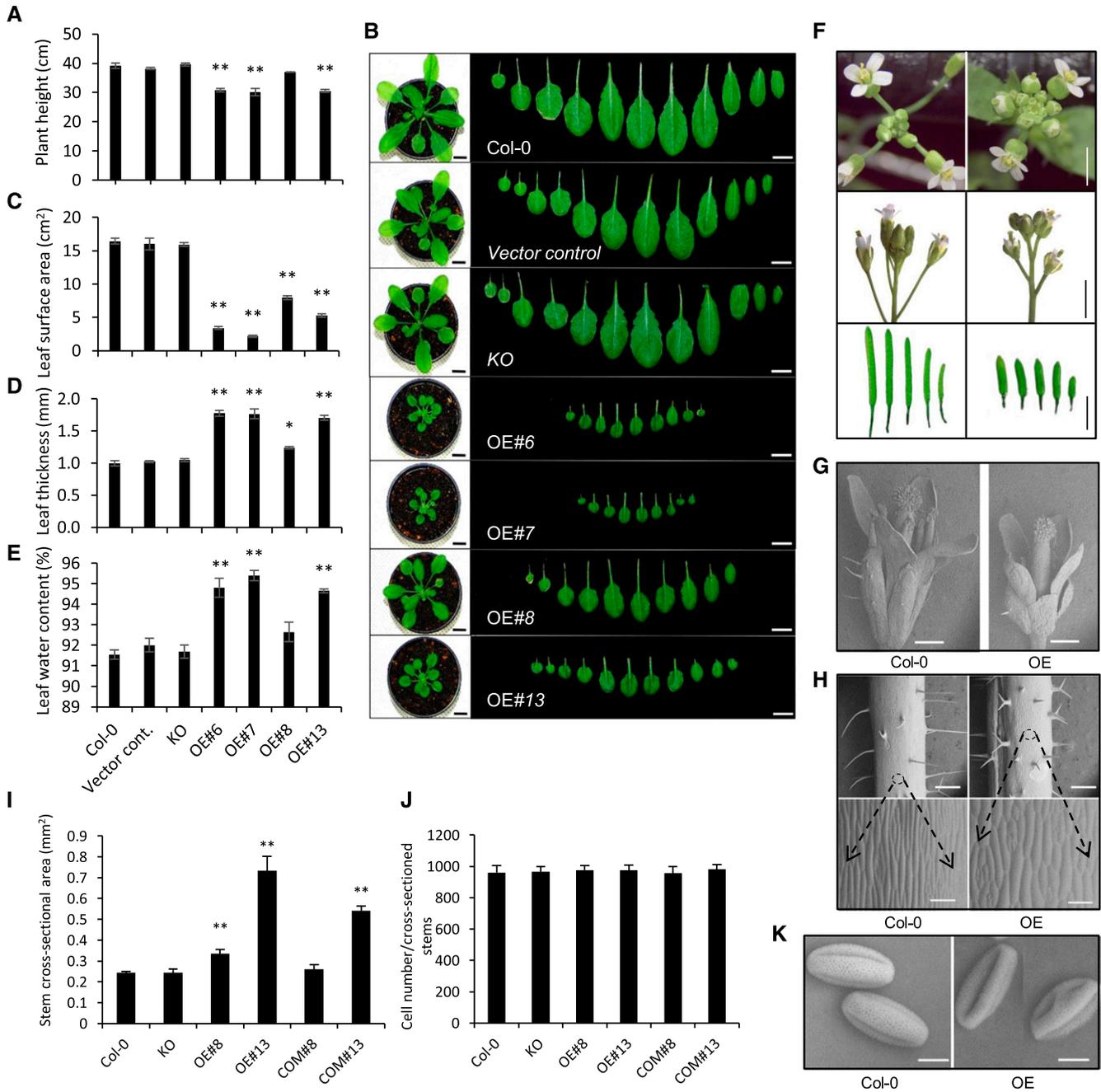
Figure 5. Overexpression of *pPLAIIIα* alters the size and shape of many cells and organs. A and C to E, Statistical analysis of plant height (A), leaf surface area (C), leaf thickness (D), and leaf water content (E) in 4-week-old plants. Mean ± SE of three independent replicates. Asterisks indicate significant difference using Student's *t* test (*$P < 0.05$ and **$P < 0.01$) compared with the controls. B, The aerial part of each 4-week-old plant with all individual leaves. The leaves are arranged from cotyledons (left) to the youngest leaves (right). Scale bars = 1 cm. F, Floral organs and siliques in the *pPLAIIIα-OE* line (13) and Col-0. Scale bars = 0.2 mm (top), 2 mm (middle), and 5 mm (lower). G, Flower in the Col-0 and *OE* lines. Scale bars = 500 μm. H, Stems in the Col-0 and *OE* lines. Scale bars = 500 μm (upper) and 100 μm (lower). I, The area (millimeters squared) of cross-sectioned stems. J, Cell number of each sectioned stems. Data represent the mean ± SD of 10 independent replicates. Asterisks indicate significant difference using Student's *t* test (**$P < 0.01$) compared with the controls. K, Pollen structures in Col-0, *KO*, and *OE* lines. Scale bars = 10 μm. All surface images were captured using a low-vacuum scanning electron microscope (model no. JSM-IT300; JEOL Korea) at a 10.8-mm working distance and 20.0 kV.
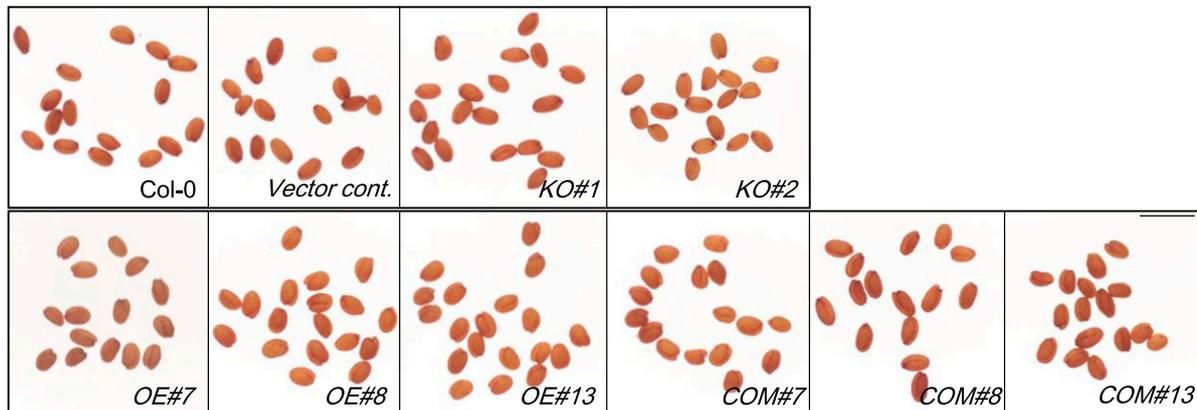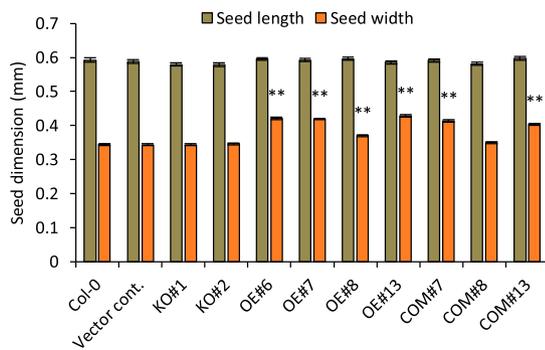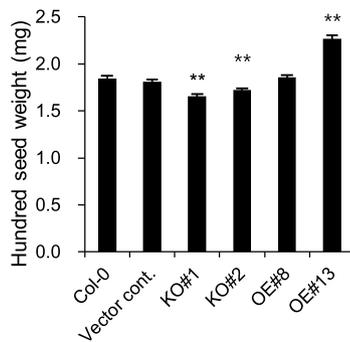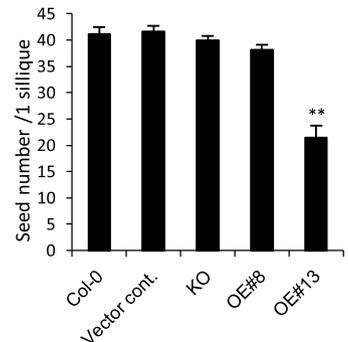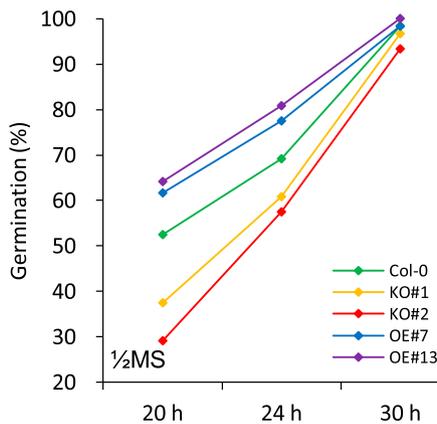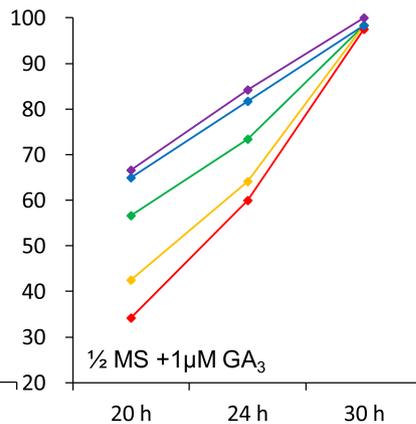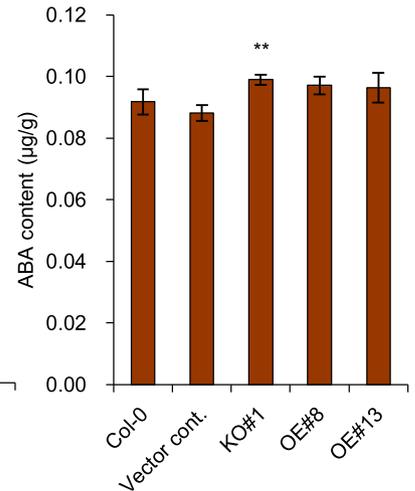
Figure 6. *pPLAIIIα* expression associates with increased germination rate and seed size. A and B, Mature seeds (A) and size (B) of control, *KO*, *OE*, and *COM* lines. Scale bar = 1 mm. Average *n* = 50 for seed size. C, The hundred-seed weight of control, *KO*, and *OE* lines. Average *n* = 10. D, Seed number per silique (*n* = 10). E and F, Germination rates of control, *KO*, and *OE* lines after 20-h germination under light conditions. *n* = 120. F, The germination rate after treatment with 1 μM of GA$_3$. G, ABA content was analyzed using UPLC. Mean $\pm$ SE (SE) of three independent replicates. Asterisks indicate significant difference using Student's *t* test (*$P < 0.05$ and **$P < 0$.) compared with the controls. 1/2 MS, One-half stregth Murashige and Skoog.

Figure 7. The mRNA levels of ethylene and GA biosynthesis genes in *pPLAIIIα-OE* lines. A and B, Gene expression patterns of *ACO*s (A) and of gibberellin oxidases (*GA2ox1, GA2ox2, GA3ox1,* and *GA20ox1*; B) from control, *KO,* and *OE* seeds imbibed for 20 h. Mean ± SE (SE) of three independent replicates. Asterisks indicate significant difference using Student's *t* test (**P* < 0.05 and ***P* < 0.01) compared with the controls.
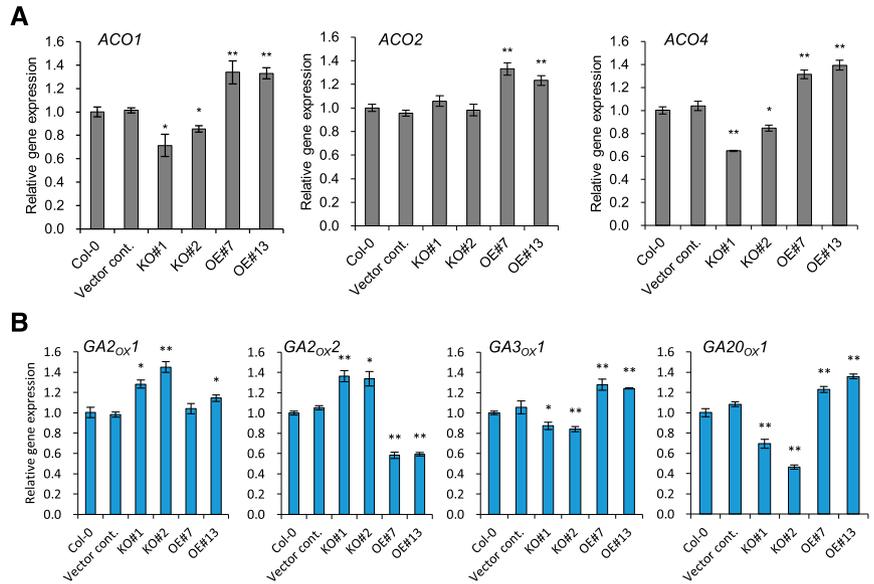
decreased in *OE* line 13. The 2-fold increase in *PR1* gene expression in the *KO* mutant and *OE* lines may be explained by two endogenous antagonistic plant hormones. SA content was higher in the *KO* mutant and *OE* line 13 compared with the controls (Fig. 9F). This finding indicates that both SA level and *PR1* gene expression are modulated by the threshold level of relative *pPLAIIIα* expression or activity in response to developmental and environmental cues. However, the endogenous JA level was two times higher in the mutant and 25% lower in *OE* lines compared with that in the controls (Fig. 9G). Thus, differential cellular levels of SA and JA seem to be coordinately involved in TCV resistance due to the function of *pPLAIIIα*.

DISCUSSION

While the molecular and biochemical functions of *pPLAIIIβ* and *pPLAIIIδ* have been characterized in Arabidopsis (Li et al., 2011, 2013), *pPLAIIIα* has only been studied in rice (Liu et al., 2015). Here, we characterized
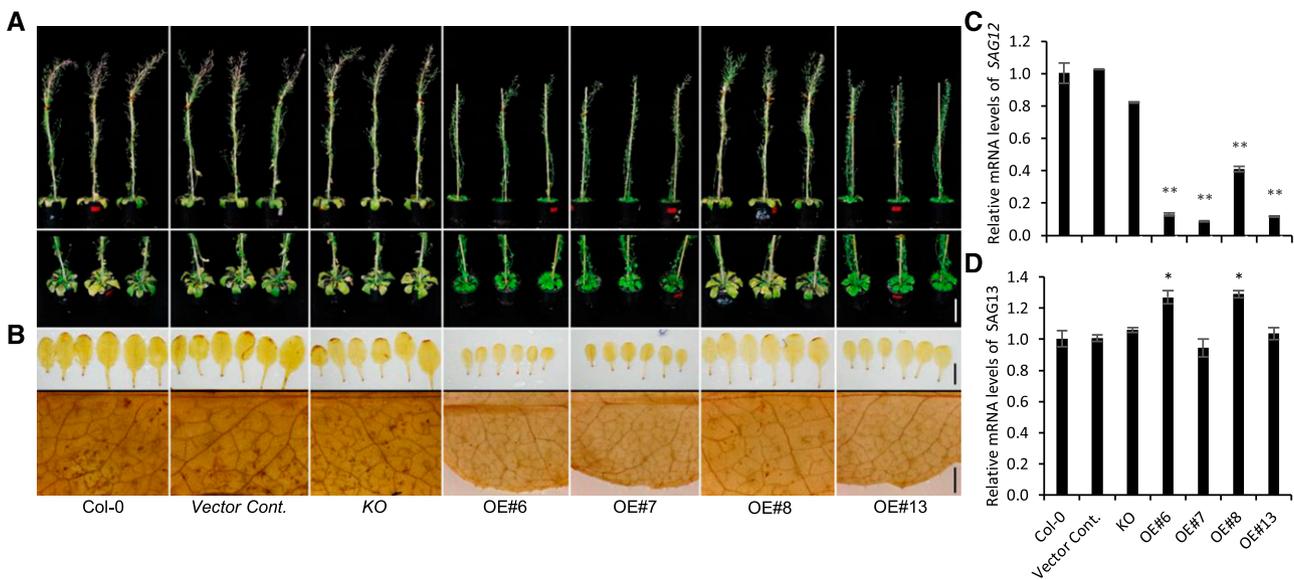
Figure 8. *pPLAIIIα-OE* lines remain green longer with reduced H_2O_2. A, Eight-week-old plants of the control, *KO,* and *pPLAIIIα-OE* lines. Scale bar = 5 cm. B, The sixth or seventh leaves were detached from 4-week-old plants and used for DAB staining. Scale bars = 1 cm. C and D, Relative gene expression patterns of two senescence marker genes, *SAG12* (C) and *SAG13* (D). Mean ± SE (SE) of three independent replicates. Asterisks indicate significant difference using Student's *t* test (**P* < 0.05 and ***P* < 0.01) compared with the controls.
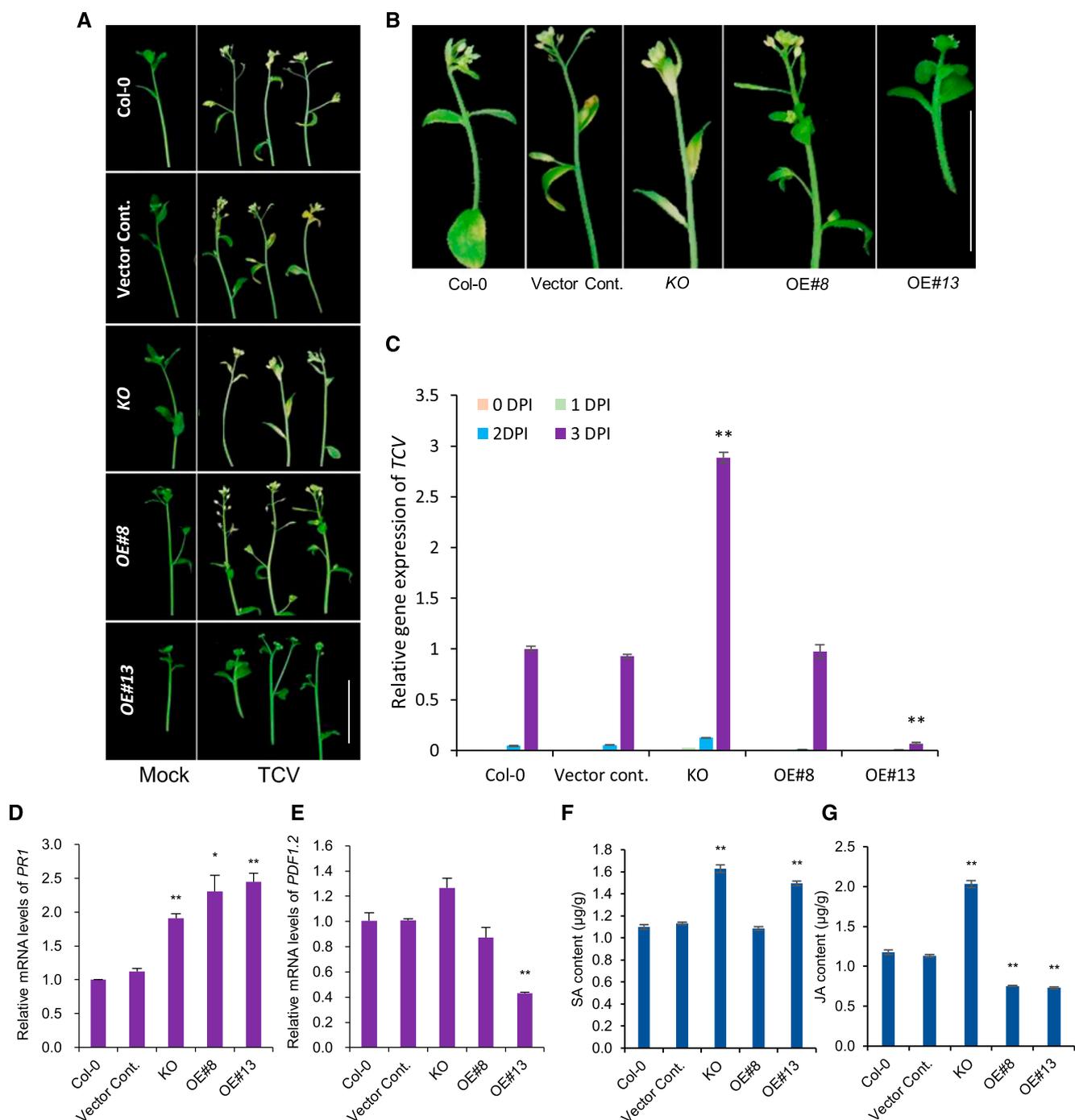
Figure 9. Increased SA in *pPLAIIIα-OE* enhances TCV resistance by changing transcript levels of *PR1* and *PDF1.2*. A, Inflorescences of each line 12 DPI of mock and TCV. B, Magnified images of TCV infected plants from each line. Scale bars = 2 cm. C to E, The relative gene expression of *TCV*, *PR1*, and *PDF1.2* in the inoculated leaves of TCV- and mock-infected plants. The inoculated leaves were monitored for the presence or absence of the HR, and RNA was extracted from inoculated leaves on 0 (1 h), 1, 2, and 3 DPI. Expression of *PR1* and *PDF1.2* was analyzed from the leaves at 1 DPI only. F and G, Hormone contents of SA and JA as measured by UPLC in rosette leaves of 5-week-old plants in control, *KO*, and *OE* lines. C to G, Four-week-old seedlings were used for the analysis. Mean ± sᴇ (sᴇ) of three independent replicates. Asterisks indicate significant difference using Student's *t* test (*$P < 0.05$ and **$P < 0.01$) compared with the controls.

pPLAIIIα KO and OE lines in Arabidopsis at the biochemical, morphological, and physiological levels. Phenotypes that confirm and extend those reported in rice were observed, such as reduced longitudinal growth and enlarged seed width and a strong relative decrease in the contents of PA as well as most other polar glycerolipid classes. But we also provide evidence for the association of pPLAIIIα with new processes, such as seed germination and virus resistance, and we give new molecular insights into pPLAIIIα signaling via regulation of expression of PLD genes.

Lipid Substrates of pPLAIIIα In Vivo

OE of Arabidopsis pPLAIIIβ increases all lipid species analyzed: phospholipids, including PE, PC, phosphatidylinositol (PI), phosphatidylserin, PA, and PG; and galactolipids, including MGDG and DGDG (Li et al., 2011). Similarly, overexpression of Arabidopsis pPLAIIIδ also tends to increase the levels of lipid species, including seed lipid reserves (Dong et al., 2014; Li et al., 2015). These counterintuitive results showing increased lipid content in plants overexpressing lipid-degrading enzymes may be explained by the fact that pPLAIIIβ may normally act in acyl editing mechanisms involved in lipid biosynthesis. Acyl editing mechanisms involve the removal by phospholipases of specific fatty acids from membrane phospholipids (for example, PC) to yield lysophospholipids and a pool of acyl-CoAs enriched in specific fatty acids that are used for synthesis of other lipids such as storage lipids (Bates et al., 2012). Increasing the pool of acyl editing-involved lysophospholipids through overexpression of specific phospholipases may create an imbalance in membrane lipid composition. This imbalance may in turn trigger an increased flux of de novo fatty acid and membrane lipid synthesis and eventually result in an overall accumulation of lipids.

By contrast, Arabidopsis pPLAIIIα-OE displayed reduced levels of many molecular lipid species compared to wild type (Fig. 4; Supplemental Fig. S4). Thus, it seems that pPLAIIIα overexpression does not act on the same mechanisms that are altered by pPLAIIIβ and pPLAIIIδ overexpression (possibly acyl editing cycles, as discussed before). This idea is consistent with the fact that lysophospholipids, which are key players in acyl editing mechanisms, accumulate in pPLAIIIβ-OE and pPLAIIIδ-OE but not in pPLAIIIα-OE. Interestingly, despite the decrease in many lipid species in the OE lines, FFAs did not accumulate in these lines compared to wild type, which showed that the FA breakdown machinery was not overwhelmed by the overexpression of pPLAIIIα. Therefore, the phenotypes observed in the OE lines are not likely caused by an excess of FFAs. Some of these phenotypes may result from the decrease in one or several of the many molecular lipid species significantly affected in both OE lines (Fig. 4; Supplemental Fig. S4). The fact that the Arabidopsis protein localizes to the PM suggests that pPLAIIIα acts

directly on phospholipid molecular species and indirectly on plastidial lipid species such as galactolipids, sulfolipids, or PG. Concerning the major plastidial lipids MGDG and DGDG, it should be noted that in OE lines the decrease in their molecular species impacts similarly both prokaryotic and eukaryotic species (Fig. 4C; Supplemental Fig. S4) and does not affect the mol % fraction (Supplemental Fig. S5) of these classes. It is thus likely that the pPLAIIIα activity in extraplastidial membranes of OEs has an indirect effect on the overall content in chloroplast membranes, but does not compromise lipid homeostasis in these organelles.

In vitro assays on the partially purified pPLAIIIα showed that the protein hydrolyzed various phospholipids, with a slightly higher activity on PA (Fig. 1B). This seems to be consistent with a decrease in all phospholipid classes with a stronger reduction in PA molecular species in OE lines (Fig. 4C). Measurement of total phospholipase activities in plant extracts did not yield further insight into pPLAIIIa in vivo activity, as no difference could be detected between wild-type and OE lines using four different phospholipid substrates (Supplemental Fig. S9). This result was possibly due to highly active phospholipases other than pPLAIIIa, or to the presence of inhibitors of pPLAIIIa activity in the extract.

In vitro activity assays and lipidomic analyses show that pPLAIIIα protein is therefore probably a nonspecific phospholipase A acting on a variety of phospholipids in the PM, with a possible slight preference for PA.

PA Levels and PLD Expression

PA accumulates at significant levels at the PM in Arabidopsis (Platre et al., 2018). The possibility that PA is one of the phospholipid classes targeted by pPLAIIIα in wild-type plants is supported by the slight preference of pPLAIIIα for PA in in vitro assays (Fig. 1C) and the strong reduction of almost all PA lipid species observed in Arabidopsis pPLAIIIα-OE (Fig. 4). These results on Arabidopsis and the previous observation in rice that a preferential decrease in PA occurs when OspPLAIIIα is overexpressed (Liu et al., 2015) thus support the view that PA is one of the possible substrates of pPLAIIIα in wild-type plants of both organisms. However, it should be stressed that hydrolysis of other phospholipid classes by Arabidopsis pPLAIIIα in vivo cannot be ruled out, because lipid species from other phospholipid classes are also reduced in OE lines (Fig. 4).

Intriguingly, no increases in PA molecular species were detected in pplaIIIa mutants in rice (Liu et al., 2015) or Arabidopsis (Fig. 4). Because PA is mostly generated by the activation of PLD (Sang et al., 2001), we checked the expression of several PLD isoforms in the Arabidopsis pplaIIIα KO mutants. Interestingly, the expression of the major PLD isoforms PLDα1, PLDζ1, and PLDζ2 decreased significantly compared to the controls in the mutant seedlings (Supplemental Fig. S10). Taken

together, these data thus suggest that pPLAIIIα hydrolyzes PA in Arabidopsis wild-type plants and that absence of this activity in the *pplaIIIα KO* results in decreased expression of several *PLD* genes to possibly maintain PA levels in the PM. Other PA-producing pathways, such as DAG phosphorylation, could also be involved and may warrant further investigation. However, in *OE* lines, the situation is clearly more complex than a simple counterbalance of PA levels by modulation of *PLD* expression. Indeed, in *OEs* there was an increase in expression of *PLD* genes only in the stronger *OE* line, while other ones showed even a decrease in *PLD* expression. Complexity of the response observed in *OEs* may be enhanced by the fact that pPLAIIIα is also active on other PM phospholipids than PA, which may activate membrane homeostasis mechanisms and interfere with lipid signaling.

Role of *pPLAIIIα* in Cell Elongation and Plant Growth

OE of *pPLAIIIβ* results in shorter leaves, petioles, hypocotyls, primary roots, and root hairs compared with the wild type (Li et al., 2011), which is partly reminiscent of the phenotypic characteristics of *pPLAIIIα-OE* in Arabidopsis (Figs. 3, F–H, and 5; Supplemental Figs. S5 and S6). Conversely, the recessive rice mutant *dep3* defective in *OspPLAIIIδ* displays a taller plant stature (Qiao et al., 2011). Generally, short and stunted morphology is observed in *pPLAIIIδ-OE* in camelina (*Camelina sativa*; Li et al., 2015), *pPLAIIIδ-OE* in Arabidopsis and *Brassica napus* (Dong et al., 2014), *pPLAIIIβ-OE* in Arabidopsis (Li et al., 2011), *OSAG78-OE* (*OnpPLAIIIδ-OE*) in Arabidopsis (Lin et al., 2011), *OspPLAIII-OE* in rice (Liu et al., 2015), and *PgpPLAIIIβ* in Arabidopsis and poplar (*Populus alba* × *Populus glandulosa*; Jang et al., 2019; Jang and Lee, 2020a). Because *pPLAIIIβ-OE* and *pPLAIIIδ-OE* show accumulation of lysolipids and FFAs, which have deleterious effects on cell membranes, it is tempting to think that the stunted phenotypes of *pPLAIII-OEs* are caused by the accumulation of pPLAIII products, which are deleterious to cellular activities. However, our data show clearly that *pPLAIIIα-OE* have stunted phenotypes in the absence of accumulation of FFAs or lysolipids. These results thus suggest that *pPLAIIIs*, at least *pPLAIIIα*, are involved in plant growth and development through the modulation of minor membrane lipid species (such as PA for pPLAIIIα) rather than via large changes in FFAs. Modified PA levels by pPLAIIIα may indirectly regulate cell elongation and plant growth, for example by affecting subcellular localization of regulatory proteins (Yao et al., 2013).

Trichomes are the outermost epidermal cells, which develop on almost all aerial structures of Arabidopsis. The *pPLAIIIα*-induced changes in trichome branching (Supplemental Fig. S7B) and pollen structure (Fig. 5K) might also be caused by altered patterns of epidermal cell elongation. Endogenous JA content is involved in trichome patterning (Yoshida et al., 2009). Overexpression

of *pPLAIIIα* reduced the level of JA content (Fig. 9G). Thus, it will be interesting to further investigate how *pPLAIIIα*-mediated lowered JA affects the trichome branching patterning.

Role of *pPLAIIIα* in Seed Germination

Overexpression of rice *pPLAIIIa* in rice (Liu et al., 2015) and Arabidopsis *pPLAIIIδ* in camelina (Li et al., 2015) thickened seed widths, but the length of seeds was reduced or not changed significantly. The recessive rice mutant *dep3*, where part of the *pPLAIIIδ* gene is deleted, shows smaller and rounder seeds but greater grain yields than control (Qiao et al., 2011). Seed sizes and weights can affect germination, but no study has yet been reported from *pPLA* gene families. Here, we show that alteration of seed morphology and weight can delay germination among *pPLAs* (Fig. 6). The importance of the plant hormone GA in promoting seed germination is well known, and ABA can act antagonistically. Ethylene also regulates germination and dormancy of many species via complex hormonal signaling networks (Corbineau et al., 2014). The knockout *pplaIIIα* mutant contained more ABA and increased gene expression of *GA2ox1*, which is involved in GA inactivation (Fig. 7B). The overexpression of *pPLAIIIα* displayed more transcripts of *GA oxidases*, which catalyze bioactive GA (Fig. 7B). Ethylene stimulates seed germination by affecting GA biosynthesis or signaling. Thus, the alternation of *pPLAIIIα* delays initial germination speed, possibly by modulating active and nonactive forms of GA, and increasing ethylene biosynthesis.

Reduced PA and JA Levels May Explain the Low Level of ROS in *pPLAIIIα-OE*

Characteristic features of leaf senescence are the ordered disassembly of the altered photosynthetic apparatus and the loss of chlorophyll (Yoshida 2003). Expression of a well-studied senescence-response gene, *SAG12*, markedly decreased in all *pPLAIIIα-OE* lines (Fig. 8C); the higher the expression of *pPLAIIIα*, the greater the reduction in *SAG12* transcripts. Suppression of *PLDα* leads to reduced superoxide synthesis via reduction in the minor phospholipid class PA (Sang et al., 2001). In addition, the formation of PA leads to the production of other lipid messengers, such as JA (Wang et al., 2000). Thus, reduced content of PA (Fig. 4C) and JA (Fig. 9G) due to the overexpression of *pPLAIIIα* could be one possible reason for the reduction in H_2O_2. Mostly reduced transcript levels of *PLD* genes in *pPLAIIIαOE* lines (Supplemental Fig. S10) should support this notion. Although *PLDα1* was slightly upregulated, other *PLDs* were all downregulated. Alternation of lipid species by the reduction of lysolipids and FFAs (Fig. 4) and hormonal signaling, such as auxin, ethylene, and GAs (Figs. 6 and 7),

could also affect the level of ROS (Corbineau et al., 2014).

A Higher SA to JA Ratio May Increase the Resistance of pPLAIIIα-OE to TCV

Some evidence suggests that at least one member of the pPLAI and pPLAII subclasses is involved in plant defenses. pplaI mutants are more sensitive to *Botrytis cinerea* infection without altering JA levels (Yang et al., 2007), whereas pPLAIIα-deficient mutants are more resistant to *Botrytis* spp. or avirulent *Pseudomonas syringae* infection (La Camera et al., 2005). Among three isoforms, pPLAIIIα, pPLAIIIβ, and pPLAIIIδ, only pPLAIIIβ is upregulated upon *Botrytis* spp. and *P. syringae* infection (La Camera et al., 2005). However, there is no clear evidence of the involvement of pPLAIII genes in plant innate immunity. Here we found that higher expression of pPLAIIIα confers TCV resistance via the regulation of SA and JA (Fig. 9). Increased levels of SA with decreased levels of JA may play crucial roles. In Col-0 and the vector control, the ratio of SA/JA was ~0.9 and 1, respectively. In KO mutants, this ratio reduced to 0.8 whereas it increased 1.4- to 2-fold in two pPLAIIIα-OE lines, 8 and 13, respectively (Fig. 9, F and G), which indicates a 2-fold higher SA level compared to the JA level in TCV resistance. During TCV infection, the HR is reportedly mediated by increased expression of defense genes, such as pathogenesis-related genes, and the accumulation of SA, phytoalexin, and camalexin (Dempsey et al., 1993; Kachroo et al., 2000). The 2.5-fold increase in PR1 expression and ~50% reduction in PDF1.2 expression mediated by SA might have increased TCV virus resistance.

MATERIALS AND METHODS

Plant Materials and Growth Conditions

Arabidopsis (*Arabidopsis thaliana*; Col-0) was used as the wild-type plant. The pplaIIIα knockout mutants (KO 1: SAIL830G12 and KO 2: SALK_040363) were purchased from the stock center (http://www.arabidopsis.org/). Seeds were maintained as reported in Jang and Lee (2020a, 2020b).

Transgene Constructs and Arabidopsis Transformation

The modified pCAMBIA1390 vector containing the CaMV 35S promoter, YFP, and/or mRFP was used (Lee et al., 2010) to express pPLAIIIα. The full pPLAIIIα genomic fragment was amplified using primers containing SalI and AvrII sites (Supplemental Table S1). Enzyme-digested PCR products were cloned into the vector (Pro-35s: pPLAIIIα-YFP/mRFP). The promoter::GUS fusion construct was generated based on the obtained upstream intergenic region of pPLAIIIα. The promoter region was amplified using primers as follows: 5′-TC CTG CAG ATC ATC AAT GTA GTC GAA-3′ (forward) and 5′-TC GTC GAC TTG CAT CGT AGT TAA CAT-3′ (reverse). The amplified PCR product was subsequently cloned into a pCAM1390 vector containing a gusA reporter gene. All transgene-confirmed constructs were transformed into Arabidopsis using *Agrobacterium tumefaciens* C58C1 (pMP90; Bechtold and Pelletier, 1998). Col-0 and the empty vector line were used as controls for the pplaIIIα mutant and pPLAIIIα-OE, respectively.

GUS Histochemical Analysis

Histochemical GUS staining was performed by incubating Prop-PLAIIIα::GUS transformants in staining buffer following Kim et al. (2014). Seedlings were photographed under a microscope (Axio Observer D1; Zeiss).

Observation of Reporter Gene Expression

Fluorescence was observed by confocal laser scanning microscopy (model no. TCS SP5 AOBS/Tandem; Leica). YFP and mRFP were detected using 514/>530 nm, and 543/560-nm to 615-nm excitation/emission filter sets, respectively. The images were acquired at the Korea Basic Science Institute, Gwangju. Korea.

Gene Expression Analysis by Reverse Transcription Quantitative PCR

Total RNA extraction, quantification of total RNA, synthesis of complementary DNA (cDNA), and reverse transcription quantitative PCR (RT-qPCR) were performed following Jang and Lee (2020a, 2020b). Three independent experiments were performed for each primer set (Supplemental Table S1).

Lipid Extraction and Lipidomic Analysis

Total lipids were extracted using the following hot isopropanol method. Briefly, 3-week–old Arabidopsis rosettes were cut, immediately weighed, and placed in 2 mL of boiling isopropanol (85°C) containing 0.01% (w/v) butylated hydroxytoluene. After 10-min heating, samples were cooled down to room temperature, and 1 μg of each internal standard was added (PE 17:0/17:0, MGDG 18:0/18:0, and TAG 17:0/17:0/17:0). Samples were then ground for 1 min using an Ultra-Turrax T25 apparatus (IKA Labortechnik), and 3 mL of methyl tert-butyl ether was added. After vortexing for 30 s, 1 mL of water was added and the mixture was shaken vigorously for 30 min and allowed to phase-separate by centrifugation at 3,000g for 2 min. The uppermost (organic) phase was collected, and 1 mL of methyl tert-butyl ether was added to the remaining lower phase. The mixture was shaken for 30 s and allowed to phase-separate by centrifugation. The upper phase was then combined with the previous organic phase, and the solvent of the total lipid extract was evaporated to dryness under a gentle stream of nitrogen gas. The total lipid extract was resuspended in 200 μL of acetonitrile/isopropanol/ammonium formate (65:30:5, v/v/v, final concentration of ammonium formate was 10 mM) and kept at −20°C until use. Quality control (QC) samples were prepared for data quantification by pooling aliquots of the lipid extract samples from Col-0 plants to make a QC stock solution. QC samples were evaporated to dryness under a gentle stream of nitrogen gas and resuspended in 200 μL of the same acetonitrile/isopropanol/ammonium formate mixture used for samples. A QC sample contained, in addition to the three internal standards coming from samples, the following quantification standards added in the molar proportions: PG (17:0/17:0), 4; PA (17:0/17:0), 1; PE (17:0/17:0) 2; PC (17:0/17:0), 4; PI (17:0/14:1), 1; MGDG (18:0/16:0), 28; DGDG (18:0/16:0), 12; SQDG (16:0/18:3), 2; LysoPG (17:1), 1; LysoPE (17:1), 1; LysoPC (17:0), 1; and FFA (17:0), 1 (purity of standards was determined before use by LC-MS/MS analysis). Samples and QC samples were subjected to ultra-performance liquid chromatography (UPLC)-MS/MS analyses using an Ultimate RS 3000 UPLC system (Dionex) connected to a quadrupole-time-of-flight 5600 mass spectrometer (AB Sciex). Samples were run in negative mode. Lipids were separated using a C8 2.1 × 150 mm, 2.6-μm column (Kinetex) and a binary gradient of solution A (60v:40v water/acetonitrile) and solution B (90v:10v isopropanol/acetonitrile). Elution was achieved through a gradient of solution B from 27% to 97%, as compared to solvent A within 20 min at a speed of 0.3 mL min^{-1}, and then at 97% for 5 min. Solution B was then decreased to a 27% enrichment during 7 min for column reequilibration. Relative quantification of lipid molecular species in samples was achieved with the software MULTIQUANT (AB Sciex) using intensity values obtained by extracting masses of the different lipids previously identified, and by normalizing based on rosette FW and the internal standard (to control for lipid extraction). In samples, absolute amounts of lipid molecular species (picomole per milligram FW) in each lipid class were estimated using intensities of the corresponding quantification standards of the QC samples (normalized by the internal standard). For lysoMGDGs and lysoDGDGs, estimates were based on one of the lysolipid standards (LPE). The estimated absolute amounts of lipid molecular species were used to calculate total amounts in each lipid class, total lipid amounts, and lipid class compositions in each line.

Protein Purification/Extraction, and Immunoblotting

The full-length cDNA of *pPLAIIIα* was cloned into the pET28a vector with the 6×His. The BL21 (DE3) bacteria expressing pPLAIIIα-His fusion protein were induced with 1 mM of isopropyl 1-thio-β-D-galactopyranoside, and the fusion protein was purified. The bacterial pellet was resuspended in lysis buffer (50 mM of NaH$_2$PO$_4$, 300 mM of NaCl, 10 mM of imidazole 1% [v/v] Triton X-100, adjusted pH to 8.0) containing 1 mg mL^{-1} of lysozyme and 1 mM of phenylmethanesulfonyl fluoride. The suspension was sonicated. After centrifugation at 10,000*g* for 20 min, the supernatant was mixed with Ni-NTA agarose resin (10% [w/v]; Qiagen). The fusion proteins bound to agarose beads were washed with washing buffer (50 mM of NaH$_2$PO$_4$, 300 mM of NaCl, and 20 mM of imidazole, adjusted pH to 8.0), and pPLAIIIα proteins were eluted with elution buffer (50 mM of NaH$_2$PO$_4$, 300 mM of NaCl, and 250 mM of imidazole, adjusted pH to 8.0). The proteins from 7-d-old seedlings were extracted using extraction buffer (120 mM of Tris-HCl at pH 7.5, 100 mM of EDTA, 5% [v/v] glycerol, 2% [w/v] SDS, 1% [v/v] Triton X-100, 300 mM of NaCl, 1 mM of dithiothreitol, and 1 mM of phenylmethanesulfonyl fluoride) after sonication and centrifugation in the same condition as for the above protein purification. The amount of purified protein was measured with the Bradford method (Bradford, 1976). The immunoblotted membranes were preblotted with 5% (v/v) skim milk for 30 min and incubated with 6×-His tag antibody, horseradish peroxidase (MA1-135; Invitrogen) for 14 h at 4°C. Anti-RFP polyclonal antibody and goat anti-Rabbit IgG (H+L) horseradish peroxidase were used as primary and secondary antibody, respectively, for *pPLAIIIα*-mRFP detection. Bands were visualized by exposing to the HR-A x-ray film after treatment with enhanced chemiluminescence substrate (Thermo Fisher Scientific).

In Vitro Enzymatic Assays

Phospholipids (each 16:0-18:1 PA, PC, PE, and PG) were purchased from Avanti Polar Lipids. Acyl hydrolyzing activities were assayed in a reaction mixture (25 mM of HEPES at pH 7.5, 10 mM of CaCl$_2$, and 10 mM of MgCl$_2$). Each 0.5 mM of lipids was used as substrate and 0.1 μg of purified protein was added to the mixture in a final volume of 100 μL. The reaction samples were incubated at 30°C for 60 min. The released nonesterified free fatty acids (NEFA) products were measured with a NEFA-HR colorimetric kit (Wako Pure Chemicals, http://www.wako-chem.co.jp/english/) using an Epoch microplate spectrophotometer (BioTek) at 546 nm.

3,3′-Diaminobenzidine Staining

For the in situ detection of H$_2$O$_2$, leaves were detached and stained with 3,3′-diaminobenzidine (DAB) solution for 4 to 5 h. DAB solution was generated by dissolving 1 mg mL^{-1} of DAB in sterile water and adjusting to pH 3.0 with 0.2 M of HCl. Additionally, 25 μL of TWEEN 20 (0.05% [v/v]) and 2.5 mL of 200 mM of Na$_2$HPO$_4$ were added. This process generated 10 mM of Na$_2$HPO$_4$ DAB staining solution and increased the pH.

TCV Infection and HR Response Analysis

Transcripts synthesized in vitro from a cloned cDNA of the TCV genome using T7 RNA polymerase were used for viral infections as described in Dempsey et al. (1993). Resistance and susceptibility were confirmed by RT-qPCR.

Phytohormone Analysis

Samples were extracted twice with ethyl acetate. The extracts were combined, evaporated, and dissolved in 70% methanol. Isotope-labeled standards (^{2}H$_4$-SA and ^{2}H$_6$-JA) were used as internal standards. UPLC (Waters) coupled with a quadrupole-time-of-flight instrument (Waters) was used for the analysis. The chromatographic separation was carried out on a C18 column. The mobile phases consisted of solvent A (0.1% [v/v] formic acid) and solvent B (acetonitrile). MS analysis was conducted in the negative ion mode with electrospray ionization.

Accession Numbers

Arabidopsis Genome Initiative locus identifiers (http://www.arabidopsis.org) for the genes described in this study are depicted in Supplemental Table S1.

Supplemental Data

The following materials are available as supplemental data.

Supplemental Figure S1. SDS-PAGE of recombinant pPLAIIIα protein.

Supplemental Figure S2. Phylogenetic tree of PLA family proteins in Arabidopsis.

Supplemental Figure S3. Transcript levels of other *pPLAIII* genes are modulated by the activity of *pPLAIIIα*.

Supplemental Figure S4. Abundance of minor lipid molecular species in MGDG, DGDG, SQDG, PG, PC, and PE lipid classes.

Supplemental Figure S5. Lipid class composition based on absolute amounts of lipid molecular species estimated by LC-MS/MS.

Supplemental Figure S6. *pPLAIIIα* expression levels affect petiole length.

Supplemental Figure S7. OE of *pPLAIIIα* affects the direction of cell elongation in filament and style and trichome length.

Supplemental Figure S8. Phenotypic differences in *KO* mutant and *OE* lines against TCV infection.

Supplemental Figure S9. Lipase activity assay using total protein from Col-0, *KO*, and *OE* plants.

Supplemental Figure S10. Relative gene expression patterns of *PLDα1*, *PLDζ1*, and *PLDζ2* in *KO* mutant and *OE* lines.

Supplemental Table S1. Primers used in confirmation of DNA insertion and PCR

LITERATURE CITED

Bates PD, Fatihi A, Snapp AR, Carlsson AS, Browse J, Lu C (2012) Acyl editing and headgroup exchange are the major mechanisms that direct polyunsaturated fatty acid flux into triacylglycerols. Plant Physiol **160:** 1530–1539

Bechtold N, Pelletier G (1998) In planta *Agrobacterium*-mediated transformation of adult *Arabidopsis thaliana* plants by vacuum infiltration. Methods Mol Biol **82:** 259–266

Bradford MM (1976) A rapid and sensitive method for the quantitation of microgram quantities of protein utilizing the principle of protein-dye binding. Anal Biochem **72:** 248–254

Corbineau F, Xia Q, Bailly C, El-Maarouf-Bouteau H (2014) Ethylene, a key factor in the regulation of seed dormancy. Front Plant Sci **5:** 539

Dempsey DA, Wobbe KK, Klessig DF (1993) Resistance and susceptible responses of *Arabidopsis thaliana* to turnip crinkle virus. Phytopathology **83:** 1021–1029

de Wit M, Galvão VC, Fankhauser C (2016) Light-mediated hormonal regulation of plant growth and development. Annu Rev Plant Biol **67:** 513–537

Dong Y, Li M, Zhang P, Wang X, Fan C, Zhou Y (2014) Patatin-related phospholipase pPLAIIIδ influences auxin-responsive cell morphology and organ size in *Arabidopsis* and *Brassica napus*. BMC Plant Biol **14:** 332

Gómez-Lim MA, Valdés-López V, Cruz-Hernandez A, Saucedo-Arias LJ (1993) Isolation and characterization of a gene involved in ethylene biosynthesis from *Arabidopsis thaliana*. Gene **134:** 217–221

Higginson T, Li SF, Parish RW (2003) AtMYB103 regulates tapetum and trichome development in *Arabidopsis thaliana*. Plant J **35:** 177–192

Holk A, Rietz S, Zahn M, Quader H, Scherer GFE (2002) Molecular identification of cytosolic, patatin-related phospholipases A from *Arabidopsis* with potential functions in plant signal transduction. Plant Physiol **130:** 90–101

Hong JK, Yun BW, Kang JG, Raja MU, Kwon E, Sorhagen K, Chu C, Wang Y, Loake GJ (2008) Nitric oxide function and signalling in plant disease resistance. J Exp Bot **59:** 147–154

Huang S, Cerny RE, Bhat DS, Brown SM (2001) Cloning of an Arabidopsis patatin-like gene, *STURDY*, by activation T-DNA tagging. Plant Physiol **125**: 573–584

Jang JH, Bae EK, Choi YI, Lee OR (2019) Ginseng-derived patatin-related phospholipase *PgpPLAIIIβ* alters plant growth and lignification of xylem in hybrid poplars. Plant Sci **288**: 110224

Jang JH, Lee OR (2020a) Overexpression of ginseng patatin-related phospholipase *pPLAIIIβ* alters the polarity of cell growth and decreases lignin content in *Arabidopsis*. J Ginseng Res **44**: 321–331

Jang JH, Lee OR (2020b) Patatin-related phospholipase *AtpPLAIIIα* affects lignification of xylem in Arabidopsis and hybrid poplars. Plants **9**: 451

Kachroo P, Yoshioka K, Shah J, Dooner HK, Klessig DF (2000) Resistance to turnip crinkle virus in *Arabidopsis* is regulated by two host genes and is salicylic acid dependent but *NPR1*, ethylene, and jasmonate independent. Plant Cell **12**: 677–690

Kim YJ, Lee OR, Oh JY, Jang MG, Yang DC (2014) Functional analysis of 3-hydroxy-3-methylglutaryl coenzyme a reductase encoding genes in triterpene saponin-producing ginseng. Plant Physiol **165**: 373–387

Kirik A, Mudgett MB (2009) SOBER1 phospholipase activity suppresses phosphatidic acid accumulation and plant immunity in response to bacterial effector AvrBsT. Proc Natl Acad Sci USA **106**: 20532–20537

Koornneef M, Bentsink L, Hilhorst H (2002) Seed dormancy and germination. Curr Opin Plant Biol **5**: 33–36

Labusch C, Shishova M, Effendi Y, Li M, Wang X, Scherer GFE (2013) Patterns and timing in expression of early auxin-induced genes imply involvement of phospholipases A (pPLAs) in the regulation of auxin responses. Mol Plant **6**: 1473–1486

La Camera S, Geoffroy P, Samaha H, Ndiaye A, Rahim G, Legrand M, Heitz T (2005) A pathogen-inducible patatin-like lipid acyl hydrolase facilitates fungal and bacterial host colonization in *Arabidopsis*. Plant J **44**: 810–825

Lee OR, Kim SJ, Kim HJ, Hong JK, Ryu SB, Lee SH, Ganguly A, Cho HT (2010) Phospholipase A₂ is required for PIN-FORMED protein trafficking to the plasma membrane in the *Arabidopsis* root. Plant Cell **22**: 1812–1825

Li M, Bahn SC, Fan C, Li J, Phan T, Ortiz M, Roth MR, Welti R, Jaworski J, Wang X (2013) Patatin-related phospholipase pPLAIIIδ increases seed oil content with long-chain fatty acids in *Arabidopsis*. Plant Physiol **162**: 39–51

Li M, Bahn SC, Guo L, Musgrave W, Berg H, Welti R, Wang X (2011) Patatin-related phospholipase pPLAIIIβ-induced changes in lipid metabolism alter cellulose content and cell elongation in *Arabidopsis*. Plant Cell **23**: 1107–1123

Li M, Wei F, Tawfall A, Tang M, Saettele A, Wang X (2015) Overexpression of patatin-related phospholipase AIIIδ altered plant growth and increased seed oil content in camelina. Plant Biotechnol J **13**: 766–778

Li-Beisson Y, Shorrosh B, Beisson F, Andersson MX, Arondel V, Bates PD, Baud S, Bird D, Debono A, Durrett TP, et al (2013) Acyl-lipid metabolism. Arabidopsis Book **11**: e0161

Lin CC, Chu CF, Liu PH, Lin HH, Liang SC, Hsu WE, Lin JS, Wang HM, Chang LL, Chien CT, et al (2011) Expression of an *Oncidium* gene encoding a patatin-like protein delays flowering in *Arabidopsis* by reducing gibberellin synthesis. Plant Cell Physiol **52**: 421–435

Linkies A, Müller K, Morris K, Turecková V, Wenk M, Cadman CSC, Corbineau F, Strnad M, Lynn JR, Finch-Savage WE, et al (2009) Ethylene interacts with abscisic acid to regulate endosperm rupture during germination: A comparative approach using *Lepidium sativum* and *Arabidopsis thaliana*. Plant Cell **21**: 3803–3822

Liu G, Zhang K, Ai J, Deng X, Hong Y, Wang X (2015) Patatin-related phospholipase A, pPLAIIIα, modulates the longitudinal growth of vegetative tissues and seeds in rice. J Exp Bot **66**: 6945–6955

Lohman KN, Gan S, John MC, Amasino RM (1994) Molecular analysis of natural leaf senescence in *Arabidopsis thaliana*. Physiol Plant **92**: 322–328

Matos AR, Pham-Thi AT (2009) Lipid deacylating enzymes in plants: Old activities, new genes. Plant Physiol Biochem **47**: 491–503

Meijer HJ, Munnik T (2003) Phospholipid-based signaling in plants. Annu Rev Plant Biol **54**: 265–306

Park CH, Roh J, Youn JH, Son SH, Park JH, Kim SY, Kim TW, Kim SK (2018) Arabidopsis ACC oxidase 1 coordinated by multiple signals mediates ethylene biosynthesis and is involved in root development. Mol Cells **41**: 923–932

Platre MP, Noack LC, Doumane M, Bayle V, Simon MLA, Maneta-Peyret L, Fouillen L, Stanislas T, Armengot L, Pejchar P, et al (2018) A combinatorial lipid code shapes the electrostatic landscape of plant endomembranes. Dev Cell **45**: 465–480.e11

Qiao Y, Piao R, Shi J, Lee SI, Jiang W, Kim BK, Lee J, Han L, Ma W, Koh HJ (2011) Fine mapping and candidate gene analysis of *dense and erect panicle 3, DEP3*, which confers high grain yield in rice (*Oryza sativa* L.). Theor Appl Genet **122**: 1439–1449

Ryu SB (2004) Phospholipid-derived signaling mediated by phospholipase A in plants. Trends Plant Sci **9**: 229–235

Sang Y, Cui D, Wang X (2001) Phospholipase D and phosphatidic acid-mediated generation of superoxide in *Arabidopsis*. Plant Physiol **126**: 1449–1458

Scherer GFE, Ryu SB, Wang X, Matos AR, Heitz T (2010) Patatin-related phospholipase A: Nomenclature, subfamilies and functions in plants. Trends Plant Sci **15**: 693–700

Thordal-Christensen H, Zhang Z, Wei Y, Collinge DB (1997) Subcellular localization of H₂O₂ in plants. H₂O₂ accumulation in papillae and hypersensitive response during the barley-powdery mildew interaction. Plant J **11**: 1187–1194

Wang C, Zien CA, Afitlhile M, Welti R, Hildebrand DF, Wang X (2000) Involvement of phospholipase D in wound-induced accumulation of jasmonic acid in *Arabidopsis*. Plant Cell **12**: 2237–2246

Wang X (2001) Plant phospholipases. Annu Rev Plant Physiol Plant Mol Biol **52**: 211–231

Wang X, Devaiah SP, Zhang W, Welti R (2006) Signaling functions of phosphatidic acid. Prog Lipid Res **45**: 250–278

Yang C, Li L (2017) Hormonal regulation in shade avoidance. Front Plant Sci **8**: 1527

Yang W, Devaiah SP, Pan X, Isaac G, Welti R, Wang X (2007) AtPLAI is an acyl hydrolase involved in basal jasmonic acid production and *Arabidopsis* resistance to *Botrytis cinerea*. J Biol Chem **282**: 18116–18128

Yao H, Wang G, Guo L, Wang X (2013) Phosphatidic acid interacts with a MYB transcription factor and regulates its nuclear localization and function in *Arabidopsis*. Plant Cell **25**: 5030–5042

Yoshida S (2003) Molecular regulation of leaf senescence. Curr Opin Plant Biol **6**: 79–84

Yoshida Y, Sano R, Wada T, Takabayashi J, Okada K (2009) Jasmonic acid control of GLABRA3 links inducible defense and trichome patterning in Arabidopsis. Development **136**: 1039–1048

Zheng Y, Li M, Wang X (2014) Proteomic insight into reduced cell elongation resulting from overexpression of patatin-related phospholipase pPLAIIIδ in *Arabidopsis thaliana*. Plant Signal Behav **9**: e28519

Zhong C, Xu H, Ye S, Zhang S, Wang X (2016) Arabidopsis seed germination assay with gibberellic acid. Bio Protoc **6**: 1–5